

First Detection of Equatorial Dark Dust Lane in a Protostellar Disk at Submillimeter Wavelength

Chin-Fei Lee,^{1,2*} Zhi-Yun Li,³ Paul. T.P Ho,^{1,4} Naomi Hirano,¹ Qizhou Zhang,⁴ Hsien Shang¹

¹*Academia Sinica Institute of Astronomy and Astrophysics, P.O. Box 23-141, Taipei 106, Taiwan*

²*Graduate Institute of Astronomy and Astrophysics, National Taiwan University, No. 1, Sec. 4, Roosevelt Road, Taipei 10617, Taiwan*

³*Astronomy Department, University of Virginia, Charlottesville, VA, USA*

⁴*Harvard-Smithsonian Center for Astrophysics, 60 Garden Street, Cambridge, MA 02138*

(Teaser) Directly detecting and characterizing small disks around the youngest protostars through high-resolution imaging with ALMA

In the earliest (so-called “Class 0”) phase of sunlike (low-mass) star formation, circumstellar disks are expected to form, feeding the protostars. However, such disks are difficult to resolve spatially because of their small sizes. Moreover, there are theoretical difficulties in producing such disks in the earliest phase, due to the retarding effects of magnetic fields on the rotating, collapsing material (so-called “magnetic braking”). With the Atacama Large Millimeter/submillimeter Array (ALMA), it becomes possible to uncover such disks and study them in detail. HH 212 is a very young protostellar system. With ALMA, we not only detect but also spatially resolve its disk in dust emission at submillimeter wavelength. The disk is nearly edge-on and has a radius of ~ 60 AU. Interestingly, it shows a prominent equatorial

dark lane sandwiched between two brighter features, due to relatively low temperature and high optical depth near the disk midplane. For the first time, this dark lane is seen at sub-millimeter wavelength, producing a “hamburger”-shaped appearance that is reminiscent of the scattered-light image of an edge-on disk in optical and near infrared. Our observations open up an exciting possibility of directly detecting and characterizing small disks around the youngest protostars through high-resolution imaging with ALMA, which provides strong constraints on theories of disk formation.

INTRODUCTION

Stars are formed inside molecular cloud cores through gravitational collapse. The details of the process, however, are complicated by the presence of magnetic fields and rotation. In theory, (rotationally supported) circumstellar disks are expected to form inside collapsing cores around protostars, feeding the protostars. Such disks have been detected with radii up to ~ 500 AU in the late (i.e., Class II or T Tauri) phases of sunlike star formation (1, 2). Such disks must have started in the earliest (Class 0) phase, as claimed in a few Class 0 sources, e.g., HH 211 (3), L 1527 (4), and recently VLA 1623 (5). However, those disks, with radii < 150 AU, have not been well resolved spatially, especially in the vertical direction, because of insufficient resolution.

In models of non-magnetized core collapse, a circumstellar disk can indeed form as early as in the Class 0 phase (6). However, a realistic model should include magnetic fields, because molecular cores are found to be magnetized (7). In the presence of a dynamically important magnetic field, when and how disks form becomes uncertain, because the field can remove angular momentum of the collapsing material efficiently, leading to the so-called “magnetic braking catastrophe” in disk formation (8). In those cases, a flattened envelope called the pseudodisk can form around the central source, but not a large rotationally supported disk (9). A misalignment between the magnetic field and the axis of rotation (10, 11) and non-ideal MHD effects (12) are sometimes able to solve this catastrophe, but not always. Even when a disk is formed, if a significant fraction of the magnetic flux of the dense core is dragged into it, the disk would rotate at a sub-Keplerian speed because of magnetic support (13).

HH 212 is a nearby protostellar system deeply embedded in a compact molecular cloud core in the L1630 cloud of Orion at a distance of ~ 400 pc. The central source is the Class 0 protostar IRAS 05413-0104, with a mass of $\sim 0.2-0.3 M_{\odot}$ (14, 15) and a bolometric luminosity $L_{\text{bol}} \sim 9 L_{\odot}$ (updated for the distance of 400 pc) (16). It is very young with an estimated age of only $\sim 40,000$ yrs (14). It drives a powerful bipolar jet (17). Accordingly to current jet models (18, 19), a circumstellar disk is required to launch the jet. Recent observations at a resolution of $\sim 0''.5$ (200 AU) shows a flattened envelope and a tentative compact disk around the central source in $\sim 850 \mu\text{m}$ dust continuum (14). The gas kinematics in HCO^+ shows that the flattened envelope is infalling with small rotation (i.e., spiraling) into the central source, which is expected for the pseudodisk in the models of magnetized core collapse (9). Inside this structure, the HCO^+ and C^{17}O kinematics indicate the presence of a rotationally supported circumstellar disk around the central source, with a radius $\lesssim 100$ AU (14, 15). Here we report ALMA observations in dust emission at $\sim 850 \mu\text{m}$ that clearly resolves the disk spatially.

RESULTS

Figure 1a shows the inner part of the jet within ~ 12000 AU ($30''$) of the source, where it was mapped in H_2 with the Very Large Telescope at $\sim 0''.35$ resolution (20) and in SiO and CO with ALMA at $\sim 0''.5$ resolution (21), in order to show the physical relationship of the envelope/disk with the jet. The jet is highly collimated with a position angle (PA) of $\sim 23^\circ$. In this figure, a reflection nebula is also seen in continuum at $2.12 \mu\text{m}$ in the infrared near the source, with a dust lane roughly perpendicular to the jet axis. This dust lane is due to dust extinction of the extended envelope detected in NH_3 (22). The jet was not detected in H_2 near the source due to the same dust

extinction. However, it was clearly detected in SiO down to the central source (Figure 1b).

At the submillimeter wavelength, dust extinction from the envelope is negligible, and thus we can detect the dust emission down to the small scales at which the circumstellar disk is formed. Previously, a flattened envelope was detected in continuum at $850 \mu\text{m}$ deep inside the extended envelope within ~ 1000 AU of the central source at $\sim 0''.5$ (200 AU) resolution (14) (Figures 1a and 1b for zoom in). Zooming into the center at a higher resolution of $\sim 0''.1$ (40 AU) (Figure 1c), we see the inner part of the envelope extending along the major axis with PA $\sim 123^\circ$ (as indicated by the white lines), roughly perpendicular to the jet axis. Zooming further into the center at an unprecedented resolution of $\sim 0''.02$ (8 AU) (Figure 1d), we see the central peak being resolved into a bright disklike structure with a major axis at PA $\sim 113^\circ$ (as indicated by the white lines), exactly perpendicular to the jet axis. At this high resolution, the noise level becomes ~ 0.08 mJy beam $^{-1}$ (see Methods), therefore, the envelope, with a flux density of < 0.11 mJy beam $^{-1}$ (estimated from Figure 1c), can not be detected. There is a big jump (by a factor of ~ 10) in the brightness temperature (hereafter T_b) from ~ 3 K (or 3 mJy beam $^{-1}$ in a $0''.1$ beam in Figure 1c) in the innermost envelope to ~ 30 K (or 1.1 mJy beam $^{-1}$ in a $0''.02$ beam in Figure 1d) in the outer part of the disklike structure, indicating that the disklike structure is physically distinct from the envelope and thus can be naturally identified as the circumstellar disk. As discussed below, since the emission in the outer disk is becoming optically thick, the density in the outer disk is expected to be more than 10 times higher than that in the innermost envelope. This jump could be due to the density jump produced by an accretion shock in disk formation (14, 23).

Being perpendicular to the jet, the disk must be nearly edge-on with the nearside tilted to the southwest, because the jet has a small inclination angle of $\sim 4\pm 2^\circ$ to the plane of the sky (24, 25), with the northeastern component tilted slightly toward us. A prominent dark lane is seen running along the major axis of the disk. The thickness of the dark lane increases with the increasing distance from the center, giving the impression that the disk is flared, although detailed modeling is required to ascertain whether this is indeed the case. A cut along the dark lane shows that the flux density increases rapidly from $\sim 0.4 \text{ mJy beam}^{-1}$ ($T_b \sim 11 \text{ K}$, 5σ) at $\sim 68 \text{ AU}$ ($0''.17$) to $\sim 1.8 \text{ mJy beam}^{-1}$ ($T_b \sim 50 \text{ K}$) at $\sim 40 \text{ AU}$ ($0''.1$), and then slowly increases to $\sim 2.1 \text{ mJy beam}^{-1}$ ($T_b \sim 58 \text{ K}$) at the center (see Figure 2), suggesting that the emission is optically thick along the dark lane, except near the edge. This suggests that mm-size particles may dominate the emission. The half-width at half maximum of the intensity profile is $\sim 60 \text{ AU}$ ($0''.15$). The dark lane is sandwiched by two brighter regions, one above at $\sim 3.3 \text{ mJy beam}^{-1}$ ($T_b \sim 90 \text{ K}$) in the northeast and one below at $\sim 2.9 \text{ mJy beam}^{-1}$ ($T_b \sim 80 \text{ K}$) in the southwest. The two regions are from the surface of the disk. They are brighter because the disk surface is expected to be warmer than the midplane, due to the heating by the radiation of the central protostar (26) and possible interaction of the disk surface with the wind from the innermost disk (27). Since the nearside of the disk is tilted slightly to the southwest, the emission in the northeast is less absorbed by the nearside of the disk and thus brighter than the emission in the southwest.

DISCUSSION

Previous observations of the disk emission at 1.4 mm and 0.85 mm suggested a spectral index of ~ 2.6 (28), and thus a dust opacity spectral index $\beta \sim 0.6$, similar to the values often obtained

for disks in more evolved (Class II) objects (29). This β indicates that grain growth to mm size or larger (30) has started early in the formation of the disk, or perhaps even before this phase, and that dust scattering is expected to contribute significantly to the disk emission in submillimeter wavelengths (31). Dust scattering should produce continuum polarization that, if detected, can provide an independent probe of the grain properties, especially their sizes (31). The total flux of the disk emission is ~ 157 mJy. If the emission is optically thin and all thermal at a temperature of 50 K, then the disk mass is $\sim 0.014 M_{\odot}$ for a dust opacity of $0.054 \text{ cm}^2 \text{ g}^{-1}$ at $850 \mu\text{m}$ (32). This estimate is quite uncertain, however, due to the large uncertainty in dust opacity and potential effects of dust scattering and because the emission in the outer disk is becoming optically thick.

To illustrate more quantitatively how the most important feature observed in HH 212, a dark lane sandwiched by two brighter regions (i.e., the “hamburger” appearance), may arise physically, we constructed a simple toy model for disk emission in submillimeter. The model is described in the supplementary materials. Briefly, the distributions of the density and temperature of the disk are prescribed, with the surface warmer than the midplane at a given radius. Figure 3 shows the emission at $850 \mu\text{m}$ for the model disk. It broadly reproduces the major features observed in the HH 212 disk, including the dark lane, the bright regions above and below the lane, with the emission above brighter than that below. In this particular example, the dark lane comes from the cooler outer part of the disk that becomes optically thick at a radius around 40 AU ($0''.1$) and the brighter emission above and below the lane is due to the warmer surfaces of the inner disk, in agreement with expectation. We refrain from drawing quantitative conclusions about the disk parameters from the model, except to note that the radius of the model disk (68 AU) is not far from that

estimated based on the intensity profile in Figure 2 (~ 60 AU) and that the disk mass ($0.05 M_{\odot}$) is also consistent with the minimum mass estimated under the optically thin assumption ($0.014 M_{\odot}$). To do better, major refinements would be needed, including a self-consistent determination of the density and temperature structures and a treatment of dust scattering, which is expected to be important for large grains.

Our observations show the first equatorial dark dust lane in a protostellar disk in the earliest phase of star formation. The detection is made possible by the unprecedented resolution achieved by ALMA long baseline. The prominent dark lane and the large brightness contrast with the envelope are strongly suggestive of the disk-like structure being a rotationally supported disk. Indeed, there is already strong indication for a Keplerian disk inside 100 AU of the protostar from molecular line observations (*14, 15*). During the earliest phase of star formation, the disks are expected to be rather small and possibly massive, which make them likely optically thick and the velocity profile difficult to measure, at least in the relatively short-wavelength ALMA bands that are needed to resolve the (small) disks. In this case, the dust continuum may be the only viable way to detect and characterize these youngest protostellar disks. Our resolved observations of HH 212 disk demonstrated that this is possible, at least for nearly edge-on systems. It raises the exciting possibility of detecting even smaller disks around deeply embedded protostars. [Note that our results of the HH 212 self-obscured disk could have general application to other Class 0 sources (*32a*)]. If small disks of tens of AUs (or smaller) turn out to be common around the earliest protostars, it would imply that the magnetic braking catastrophe in the theoretical literature of disk formation is averted early on, plausibly through non-ideal MHD effects, which are expected to be

most efficient at decoupling the magnetic field from the bulk material close to the central star where the density is the highest (33). Just as importantly, our observations open a window on the vertical structure of the disks around deeply embedded protostars in the earliest (Class 0) phase, which could ultimately be compared to those surrounding more evolved young stars (Class I sources and T Tauri stars), potentially yielding key insights on the processes of grain growth and settling that are important to planet formation.

MATERIALS AND METHODS

Observations of the HH 212 protostellar system were carried out with ALMA in Band 7 at ~ 350 GHz in Cycles 1 and 3, with 32-45 antennas and projected baselines ranging from ~ 15 to 16200 m. The total time on the HH 212 system is ~ 148 minutes. We also introduce a parametrized model for the disk emission in HH 212, in order to illustrate the formation of the dark lane sandwiched between two brighter regions. Details of our data reduction and radiative transfer modeling are provided in Supplementary Materials.

SUPPLEMENTARY MATERIALS

Materials and Methods

Table S1. Observation Logs

Table S2. Correlator Setup for Cycle 1 Project

Table S3. Correlator Setup for Cycle 3 Project

Table S4. Calibrators and Their Flux Densities

References (34-36)

REFERENCES AND NOTES

1. M. Simon, A. Dutrey, S. Guilloteau, Dynamical Masses of T Tauri Stars and Calibration of Pre-Main-Sequence Evolution. *Astrophys. J.*, **545**, 1034-1043 (2000).
2. L. M. Pérez, J. M. Carpenter, S. M. Andrews, L. Ricci, A. Isella, H. Linz, A. I. Sargent, D. J. Wilner, T. Henning, A. T. Deller, C. J. Chandler, C. P. Dullemond, J. Lazio, K. M. Menten, S. A. Corder, S. Storm, L. Testi, M. Tazzari, W. Kwon, N. Calvet, J. S. Greaves, R. J. Harris, L. G. Mundy, Spiral density waves in a young protoplanetary disk. *Science*, **353**, 1519-1521 (2016).
3. C.-F. Lee, N. Hirano, A. Palau, P. T. P. Ho, T. L. Bourke, Q. Zhang, H. Shang, Rotation and Outflow Motions in the Very Low-Mass Class 0 Protostellar System HH 211 at Subarcsecond Resolution. *Astrophys. J.*, **699**, 1584-1594 (2009).
4. J. J. Tobin, L. Hartmann, H.-F. Chiang, D. J. Wilner, L. W. Looney, L. Loinard, N. Calvet, P. D'Alessio, A ~ 0.2 -solar-mass protostar with a Keplerian disk in the very young L1527 IRS system. *Nature*, **492**, 83-85 (2012).
5. N. M. Murillo, S.-P. Lai, S. Bruderer, D. Harsono, E. F. van Dishoeck, A Keplerian disk around a Class 0 source: ALMA observations of VLA1623A. *Astron. Astrophys.*, **560**, A103(2013).
6. S. Terebey, F. H. Shu, P. Cassen, The collapse of the cores of slowly rotating isothermal clouds. *Astrophys. J.*, **286**, 529-551 (1984).

7. N. L. Chapman, J. A. Davidson, P. F. Goldsmith, M. Houde, W. Kwon, Z.-Y. Li, L. W. Looney, B. Matthews, T. G. Matthews, G. Novak, R. Peng, J. E. Vaillancourt, N. H. Volgenau, Alignment between Flattened Protostellar Infall Envelopes and Ambient Magnetic Fields. *Astrophys. J.*, **770**, 151-164 (2013).
8. Z.-Y. Li, R. Banerjee, R. E. Pudritz, J. K. Jørgensen, H. Shang, R. Krasnopolsky, A. Maury, The Earliest Stages of Star and Planet Formation: Core Collapse, and the Formation of Disks and Outflows. *Protostars and Planets*, **VI**, 173-194 (2014).
9. A. Allen, Z.-Y. Li, F. H. Shu, Collapse of Magnetized Singular Isothermal Toroids. II. Rotation and Magnetic Braking. *Astrophys. J.*, **599**, 363-379 (2003).
10. M. Joos, P. Hennebelle, A. Ciardi, Protostellar disk formation and transport of angular momentum during magnetized core collapse. *Astron. Astrophys.*, **543**, A128-A149 (2012).
11. Z.-Y. Li, R. Krasnopolsky, H. Shang, Does Magnetic-field-Rotation Misalignment Solve the Magnetic Braking Catastrophe in Protostellar Disk Formation? *Astrophys. J.*, **774**, 82-93 (2013).
12. K. Tomida, S. Okuzumi, M. N. Machida, Radiation Magnetohydrodynamic Simulations of Protostellar Collapse: Nonideal Magnetohydrodynamic Effects and Early Formation of Circumstellar Disks. *Astrophys. J.*, **801**, 117-136 (2015).
13. F. H. Shu, S. Lizano, D. Galli, M. J. Cai, S. Mohanty, The Challenge of Sub-Keplerian Rotation for Disk Winds. *Astrophys. J. Lett.*, **682**, L121-L124 (2008).

14. C.-F. Lee, N. Hirano, Q. Zhang, H. Shang, P. T. P. Ho, R. Krasnopolsky, ALMA Results of the Pseudodisk, Rotating Disk, and Jet in the Continuum and HCO⁺ in the Protostellar System HH 212. *Astrophys. J.*, **786**, 114-125 (2014).
15. C. Codella, S. Cabrit, F. Gueth, L. Podio, S. Leurini, R. Bachiller, A. Gusdorf, B. Lefloch, B. Nisini, M. Tafalla, W. Yvart, The ALMA view of the protostellar system HH212. The wind, the cavity, and the disk. *Astron. Astrophys.*, **568**, L5-L9 (2014).
16. H. Zinnecker, P. Bastien, J.-P. Arcoragi, H. W. Yorke, Submillimeter dust continuum observations of three low luminosity protostellar IRAS sources. *Astron. Astrophys.*, **265**, 726-732 (1992).
17. H. Zinnecker, M. J. McCaughrean, and J. T. Rayner, A symmetrically pulsed jet of gas from an invisible protostar in Orion. *Nature*, **394**, 862-865 (1998).
18. A. Konigl, R. E. Pudritz, Disk Winds and the Accretion-Outflow Connection. *Protostars and Planets*, **IV**, 759(2000).
19. F. H. Shu, J. R. Najita, H. Shang, Z.-Y. Li, X-Winds Theory and Observations. *Protostars and Planets*, **IV**, 789-814 (2000).
20. M. McCaughrean, H. Zinnecker, M. Andersen, G. Meeus, N. Lodieu, Standing on the shoulder of a giant: ISAAC, Antu, and star formation. *The Messenger*, **109**, 28-36 (2002).
21. C.-F. Lee, N. Hirano, Q. Zhang, H. Shang, P. T. P. Ho, Y. Mizuno, Jet Motion, Internal Working Surfaces, and Nested Shells in the Protostellar System HH 212. *Astrophys. J.*, **805**, 186-194 (2015).

22. J. Wiseman, A. Wootten, H. Zinnecker, and M. McCaughrean, The Flattened, Rotating Molecular Gas Core of Protostellar Jet HH 212. *Astrophys. J. Lett.*, **550**, L87-L90 (2001).
23. R. Krasnopolsky, A. Königl, Self-similar Collapse of Rotating Magnetic Molecular Cloud Cores. *Astrophys. J.*, **580**, 987-1012 (2002).
24. M. J. Claussen, K. B. Marvel, A. Wootten, and B. A. Wilking, Distribution and Motion of the Water Masers near IRAS 05413-0104. *Astrophys. J. Lett.*, **507**, L79-L82 (1998).
25. C.-F. Lee, P. T. P. Ho, N. Hirano, H. Beuther, T. L. Bourke, H. Shang, Q. Zhang, HH 212: Submillimeter Array Observations of a Remarkable Protostellar Jet. *Astrophys. J.*, **659**, 499-511 (2007).
26. E. I Chiang, P. Goldreich, Spectral Energy Distributions of T Tauri Stars with Passive Circumstellar Disks. *Astrophys. J.*, **490**, 368-376 (1997).
27. Z.-Y. Li, F. H. Shu, Interaction of Wide-Angle MHD Winds with Flared Disks. *Astrophys. J.*, **468**, 261-268 (1996).
28. C.-F. Lee, P. T. P. Ho, T. L. Bourke, N. Hirano, H. Shang, Q. Zhang, SiO Shocks of the Protostellar Jet HH 212: A Search for Jet Rotation. *Astrophys. J.*, **685**, 1026-1032 (2008).
29. Natta, A., L. Testi, N. Calvet, T. Henning, R. Waters, and D. Wilner, Dust in Protoplanetary Disks: Properties and Evolution. *Protostars and Planets V*, 767-781 (2007).
30. B. T. Draine, On the Submillimeter Opacity of Protoplanetary Disks. *Astrophys. J.*, **636**, 1114-1120 (2006).

31. A. Kataoka, T. Muto, M. Momose, T. Tsukagoshi, M. Fukagawa, H. Shibai, T. Hanawa, K. Murakawa, C. P. Dullemond, Millimeter-wave Polarization of Protoplanetary Disks due to Dust Scattering. *Astrophys. J.*, **809**, 78-92 (2015).
32. S. V. W. Beckwith, A. I. Sargent, R. S. Chini, R. Guesten, A survey for circumstellar disks around young stellar objects. *Astron. J.*, **99**, 924-945 (1990).
- 32a. J.I-H Li, H.B. Liu, Y. Hasegawa, N. Hirano, Systematic analysis of SED and the dust opacity indices for Class 0 YSOs. *Astrophys. J.*, *accepted*
33. T. Nakano, R. Nishi, T. Umebayashi, Mechanism of Magnetic Flux Loss in Molecular Clouds. *Astrophys. J.*, **573**, 199-214 (2002).
34. P. J. Armitage, Physical processes in protoplanetary disks. , arXiv:1509.06382(2015).
35. S. M. Andrews, D. J. Wilner, A. M. Hughes, C. Qi, C. P. Dullemond, Protoplanetary Disk Structures in Ophiuchus. *Astrophys. J.*, **700**, 1502-1523 (2009).
36. C. P. Dullemond, C. Dominik, Flaring vs. self-shadowed disks: The SEDs of Herbig Ae/Be stars. *Astron. Astrophys.*, **417**, 159-168 (2004).

Acknowledgements This paper makes use of the following ALMA data: ADS/JAO.ALMA#2012.1.00122.S and 2015.1.00024.S. ALMA is a partnership of ESO (representing its member states), NSF (USA) and NINS (Japan), together with NRC (Canada), NSC and ASIAA (Taiwan), and KASI (Republic of Korea), in cooperation with the Republic of Chile. The Joint ALMA Observatory is operated by ESO, AUI/NRAO and NAOJ.

Funding: C.-F.L. acknowledges grants from the Ministry of Science and Technology of Taiwan (MoST 104-2119-M-001-015-MY3) and the Academia Sinica (Career Development Award). Z.-Y.L. is supported in part by NSF AST1313083 and NASA NNX14AB38G, NH by MoST 105-2112-M-001-026. **Author Contributions:** C.-F.L. led the project, analysis, discussion, and drafted the manuscript. Z.-Y.L. participated in the analysis and discussion, and commented on the manuscript. All other coauthors contribute to scientific discussion. **Competing Interests:** The authors declare that they have no competing interests. **Data and materials availability:** All data needed to evaluate the conclusions in the paper are present in the paper and/or the Supplementary Materials. Our ALMA data can also be obtained from the ALMA Science Data Archive, <https://almascience.nao.ac.jp/alma-data>". Additional data available from authors upon request.

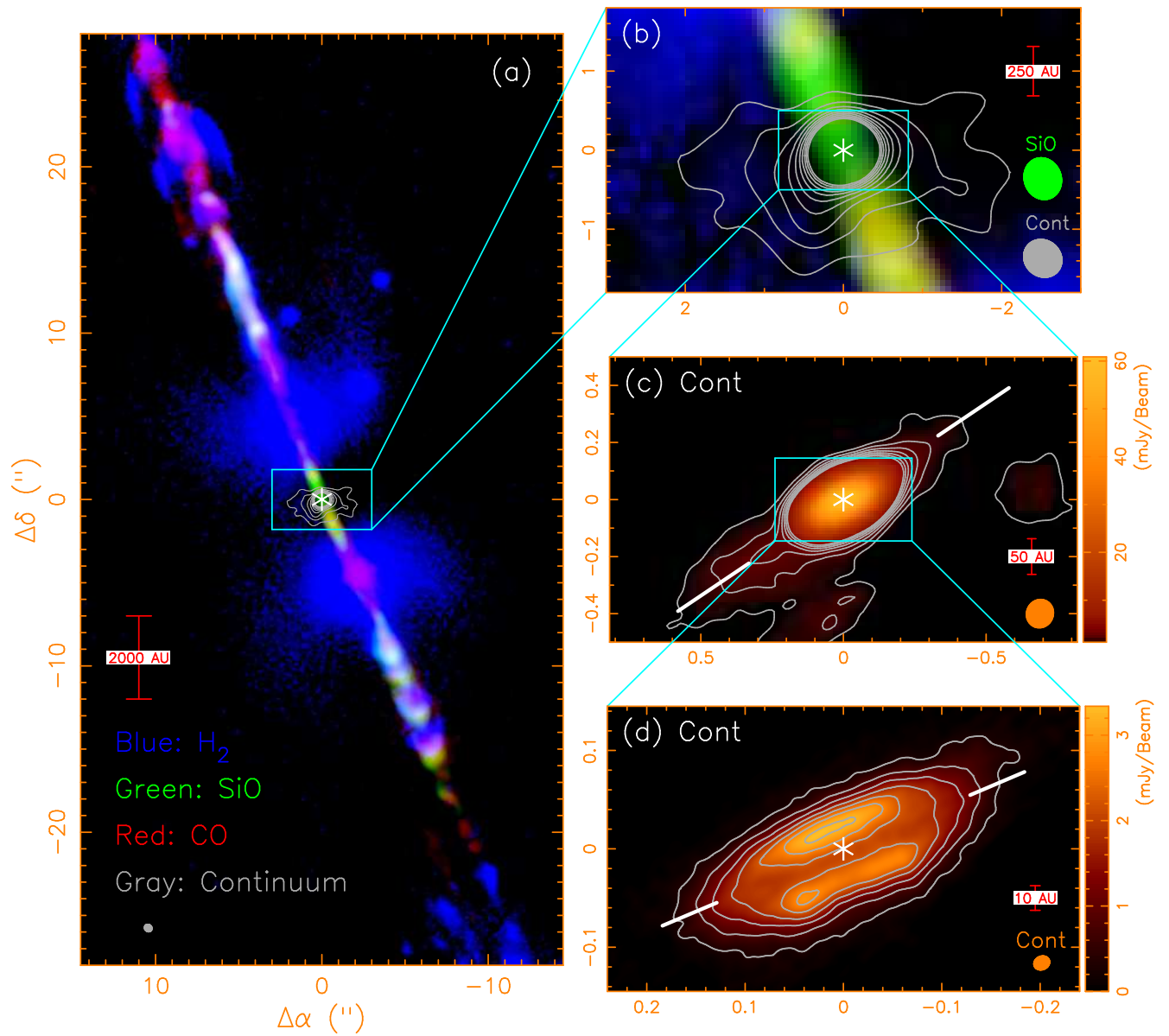


Figure 1. (a) A composite image for the inner part of the HH 212 jet: blue shows the map of H₂ + 2.12 μm continuum, obtained with the Very Large Telescope (20), green and red show the SiO and CO maps, respectively, obtained with ALMA (21). Gray contours show the continuum map of the envelope/disk at 850 μm obtained with ALMA at $\sim 0''.5$ resolution (14). Contours start at

3.125 mJy beam⁻¹ with a step of 3.75 mJy beam⁻¹. (b) A zoom-in to the center for the jet and envelope/disk. (c) A zoom-in to the center of the continuum at $\sim 0''.1$ resolution. Contours start at 1.23 mJy beam⁻¹ with a step of 0.62 mJy beam⁻¹. (d) A zoom-in to the center of the continuum at $\sim 0''.02$ resolution. Contours start at 0.29 mJy beam⁻¹ with a step of 0.49 mJy beam⁻¹. Asterisks mark the possible source position at $\alpha_{(2000)} = 05^{\text{h}}43^{\text{m}}51^{\text{s}}.4086$, $\delta_{(2000)} = -01^{\circ}02'53''.147$, obtained by comparing to the model in Figure 3.

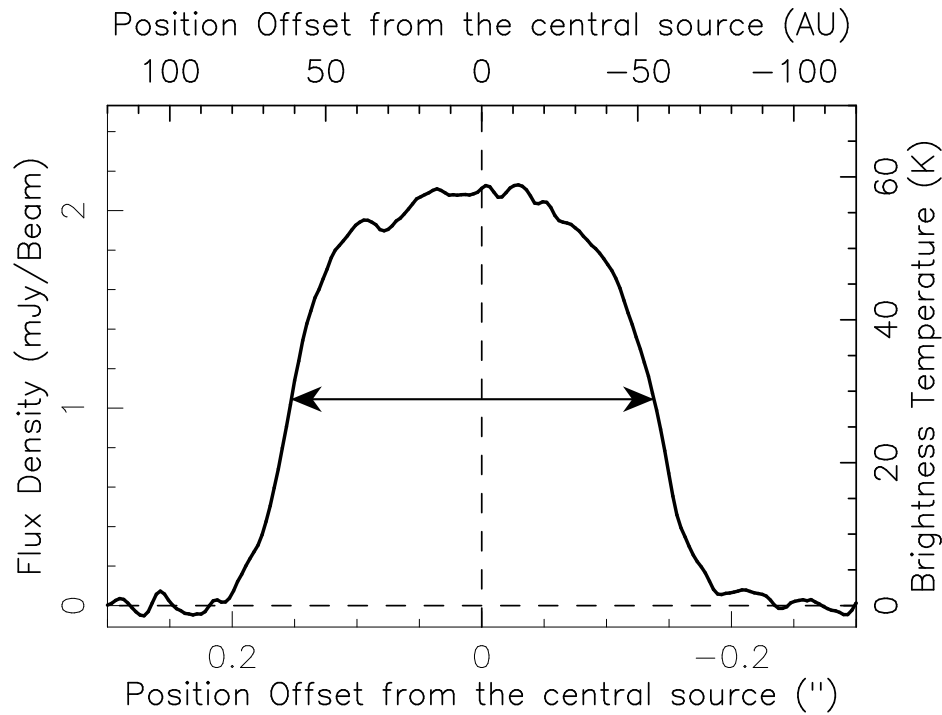


Figure 2. Flux density (and corresponding brightness temperature) of the continuum cut along the dark lane. The vertical dashed line indicates the source position. The double sized arrow marks the full-width at half maximum of the intensity profile.

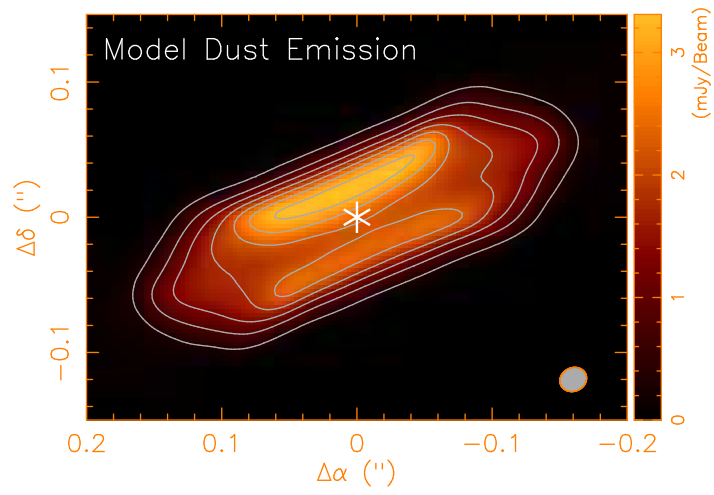


Figure 3. Simulated observed continuum emission at $850\ \mu\text{m}$ derived from the model. Contour levels are the same as in Figure 1d.

Supplementary Materials

Materials and Methods

Observations Observations of the HH 212 protostellar system were carried out with ALMA in Band 7 at ~ 350 GHz in Cycles 1 and 3, with 32-45 antennas and projected baselines ranging from ~ 15 to 16200 m (see Table S1). The Cycle 1 project was carried out with 2 executions, both on 2015 August 29 during the Early Science Cycle 2 phase. The Cycle 3 project was carried out with 2 executions in 2015, one on November 5 and one on December 3, during the Early Science Cycle 3 phase. For the Cycle 1 project, the correlator was set up to have 4 spectral windows, with one for CO $J = 3 - 2$ at 345.795991 GHz, one for SiO $J = 8 - 7$ at 347.330631 GHz, one for HCO⁺ $J = 4 - 3$ at 356.734288 GHz, and one for the continuum at 358 GHz (see Table S2). For the Cycle 3 project, the correlator was more flexible and thus was set up to include 2 more spectral windows, with one for SO $N_J = 8_9 - 7_8$ at 346.528481 GHz and one for H¹³CO⁺ $J = 4 - 3$ at 346.998338 GHz (see Table S3). The total time on the HH 212 system is ~ 148 minutes.

In this paper, we only present the observational results in continuum, which traces the envelope and disk around the central source. Line-free channels were extracted from all the spectral windows to make the continuum with a frequency centered at ~ 352 GHz (or $\sim 850 \mu\text{m}$). The data were calibrated with the Common Astronomy Software Applications (CASA) package, with quasars as bandpass, flux, and phase calibrators, as listed in Table S4 with their flux densities. Two different weightings were used to generate the continuum maps at two different resolutions. One

used a robust factor of 2 (natural weighting) with the baselines from ~ 15 to 2000 m in order to map the innermost envelope around the disk with enough sensitivity and resolution. This generates a synthesized beam (resolution) of $0''.100 \times 0''.094$ at a position angle (P.A.) of -25° and a noise level of $\sim 0.42 \text{ mJy beam}^{-1}$ (0.44 K) (Figure 1c). Another one used a robust factor of 0.5 (super-uniform weighting) with all the baselines, in order to resolve the disk structure. In addition, data from all baselines were included so that only structure with a size scale greater than $\sim 2''$ could be filtered out in our image. This generates a synthesized beam of $0''.0203 \times 0''.0175$ at a P.A. of -65° and a noise level of $\sim 0.08 \text{ mJy beam}^{-1}$ (2.2 K) (Figure 1d).

Model In this section, we introduce a parametrized model for the disk emission, in order to illustrate the formation of the dark lane sandwiched between two brighter regions.

For a disk in vertical hydrostatic equilibrium, the scale height h in the cylindrical coordinate system is given by (34)

$$\frac{h}{R} \sim \frac{c_s}{v_\phi} \propto \frac{R^{-q/2}}{R^{-1/2}} = \left(\frac{R}{R_o}\right)^{(1-q)/2} \quad (1)$$

where R is the cylindrical radius and c_s is the isothermal sound speed proportional to $T^{1/2}$, where T is the temperature. Assuming $T \propto R^{-q}$, we have $c_s \propto R^{-q/2}$. For reference, q is ~ 0.5 in Taurus disks (35) and 0.75 in geometrically thin accretion disk model (34). v_ϕ is the rotational velocity assumed to be Keplerian and thus proportional to $R^{-1/2}$, as suggested by C^{17}O gas kinematics (15). In this case, the scale height of the disk increases with the disk radius monotonically. However, the continuum map in Figure 1d appears to indicate that the disk becomes thinner near the outer edge. The physical reason for the behavior is unclear; it could be due to self-shielding (36) or optical

Table S1: Observation Logs

Cycle	Date (YYYY-MM-DD)	Array Configuration	Number of Antennas	Time on target (minutes)	Baselines (meter)
1	2015-08-29	C32-6	37	30	15–1466
1	2015-08-29	C32-6	35	30	15–1466
3	2015-11-05	C36-7/8	45	44	78–16196
3	2015-12-03	C36-7/8	32	44	17–6344

Table S2: Correlator Setup for Cycle 1 Project

Spectral Window	Line or Continuum	Number of Channels	Central Frequency (GHz)	Bandwidth (MHz)	Channel Width (kHz)
0	CO J=3-2	3840	345.803	468.750	122.070
1	SiO J=8-7	3840	347.338	468.750	122.070
2	HCO ⁺ J=4-3	3840	356.742	468.750	122.070
3	Continuum	3840	358.008	1875.000	488.281

Table S3: Correlator Setup for Cycle 3 Project

Spectral Window	Line or Continuum	Number of Channels	Central Frequency (GHz)	Bandwidth (MHz)	Channel Width (kHz)
0	SO $N_J = 8_9 - 7_8$	960	346.528	234.375	244.140
1	CO $J = 3 - 2$	960	345.796	234.375	244.140
2	H ¹³ CO ⁺ $J = 4 - 3$	960	346.998	234.375	244.140
3	SiO $J = 8 - 7$	960	347.330	234.375	244.140
4	HCO ⁺ $J = 4 - 3$	1920	356.735	468.750	244.140
5	Continuum	1920	357.994	1875.000	976.562

Table S4: Calibrators and Their Flux Densities

Date (YYYY-MM-DD)	Bandpass Calibrator (Quasar, Flux Density)	Flux Calibrator (Quasar, Flux Density)	Phase Calibrator (Quasar, Flux Density)
2015-08-29	J0607-0834, 1.20 Jy	J0423-013, 1.03 Jy	J0552+0313, 0.25 Jy
2015-08-29	J0607-0834, 1.20 Jy	J0423-013, 1.03 Jy	J0552+0313, 0.25 Jy
2015-11-05	J0423-0120, 0.55 Jy	J0423-0120, 0.55 Jy	J0541-0211, 0.22 Jy
2015-12-03	J0510+1800, 4.07 Jy	J0423-0120, 0.67 Jy	J0541-0211, 0.23 Jy

depth effects. To model the decrease of disk thickness near the edge, we introduce a radius, R_t , beyond which the scale height decreases exponentially. Let h_t be the scale height of the disk at R_t , we have

$$h(R) \sim h_t \begin{cases} (\frac{R}{R_t})^{1+(1-q)/2} & \text{if } R < R_t, \\ \exp[-(\frac{R-R_t}{R_o-R_t})^2] & \text{if } R_t \leq R \leq R_o \end{cases} \quad (2)$$

where R_o is the outer radius of the disk.

The temperature increases not only radially toward the center but also vertically from the disk midplane to the surface for a passive disk (assumed here), either because of radiative heating by the central source or mechanical heating from wind-disk interaction. The detailed temperature structure depends on many factors, such as the properties of the dust grains and their spatial distribution, which are uncertain. For illustrative purposes, we adopt

$$T \sim T_t (\frac{R}{R_t})^{-q} \begin{cases} \exp(\frac{z^2}{2h^2}) & \text{if } R < R_t, \\ 1 & \text{if } R_t \leq R \leq R_o \end{cases} \quad (3)$$

where T_t is the temperature in the disk midplane at R_t . The number density of molecular hydrogen is assumed to be (34)

$$n = n_t (\frac{R}{R_t})^{-p} \exp(-\frac{z^2}{2h^2}) \quad (4)$$

with the power-law index $p = 2$ and n_t being the number density in the disk midplane at R_t . Helium is included so that the mass density is $\rho = 1.4nm_{H_2}$.

We used our radiative transfer code to obtain dust continuum emission map from the model disk. We first computed the thermal emission from each point in the disk based on its local temperature, and then generated a synthetic map by integrating along each line of sight the local emission

that is attenuated by the optical depth. With the dust opacity spectral index $\beta \sim 0.6$ found in previous observations of the HH 212 disk (28) and the dust opacity formula for circumstellar disks (32), we derived a dust opacity $\kappa \sim 0.054 \text{ cm}^2 \text{ g}^{-1}$ at $850 \mu\text{m}$. We assume $p = 2$ and $q = 0.75$ for the disk (34). Based on the disk structure seen in the dust emission map in Figure 1d, we find that $R_o \sim 0''.17 \pm 0''.03$ ($68 \pm 12 \text{ AU}$), $R_t \sim 0''.09 \pm 0''.02$ ($36 \pm 8 \text{ AU}$), and $h_t \sim 0''.03 \pm 0''.01$ ($12 \pm 4 \text{ AU}$). To produce the image shown in Figure 3, we adopted $n_t \sim 2.2 \pm 0.6 \times 10^{10} \text{ cm}^{-3}$ and $T_t \sim 73 \pm 10 \text{ K}$. With this value of n_t , the emission becomes optically thick at $R \sim 0''.1$ (40 AU). The value of T_t yields a flux density of $\sim 2.0 \text{ mJy beam}^{-1}$ in a $0''.02$ beam (or a brightness temperature of $\sim 55 \text{ K}$) in the optically thick region, consistent with Figure 2. The disk has a total mass of

$$M_D = 1.4 m_{\text{H}_2} \int n 2\pi R dR dz \sim 0.05 M_\odot \quad (5)$$

Since part of the observed emission comes from the dust thermal emission and part from the dust scattering of the thermal emission, the disk mass derived here is likely an upper limit. Note that the mid-plane temperature of 73 K at the radius $R_t = 36 \text{ AU}$ yields an isothermal scale height of $\sim 8.3 \text{ AU}$ for an estimated central mass of $0.2 M_\odot$. This value is somewhat smaller than the best fit value of $h_t \sim 12 \text{ AU}$. The agreement between the two may be improved when the variation of temperature with height is taken into account. More detailed treatment of heating and cooling is needed to draw a firmer conclusion.